Low-Grazing Angle Scattering from Rough Surfaces in a Duct Formed by a Linear-Square Refractive Index Profile

Ra'id S. Awadallah, *Member, IEEE,* and Gary S. Brown, *Fellow, IEEE*

***Abstract*—The problem of rough surface scattering and propagation over rough terrain in a ducting environment has been receiving considerable attention in the literature. One popular method of modeling this problem is the parabolic wave equation (PWE) method. An alternative method is the boundary integral equation (BIE) method. The implementation of the BIE in inhomogeneous media (ducting environments) is not straightforward, however, since the Green's function for such a medium is not usually known. In this paper, a closed-form approximation of the Green's function for a two-dimensional (2-D) ducting environment formed by a linear-square refractive index profile is derived using asymptotic techniques. This Green's function greatly facilitates the use of the BIE approach to study low-grazing angle (LGA) rough surface scattering and propagation over rough surfaces in the aforementioned ducting environment. This paper demonstrates how the BIE method can model the combined effects of surface roughness and medium inhomogeneity in a very rigorous fashion. Furthermore, it illustrates its capability of accurately predicting scattering in all directions including backscattering. The boundary integral equation of interest is solved via the method of ordered multiple interactions (MOMI), which eliminates the requirements of matrix storage and inversion and, hence, allows the application of the BIE method to very long rough surfaces.**

***Index Terms*—Asymptotic techniques, electromagnetic (EM) scattering by rough surfaces, ducting environments, integral equation methods, nonhomogenous media, numerical methods.**

I. Introduction

DURING the past several decades, researchers in the areas of applied electromagnetics (EMs) and underwater acoustics have been searching for rigorous and efficient models for mathematically describing wave propagation over rough surfaces as well as the scattering of these waves by such surfaces. These researchers have also been interested in studying the combined effect of atmospheric conditions (ducting conditions) and surface roughness on the propagation and scattering problem. Two main methods for modeling this problem are available in the literature. These are the parabolic wave equation (PWE) and the boundary integral equation (BIE) models.

Manuscript received July 21, 1998; revised June 4, 1999. This work was supported in part by the Sensing and Systems Division of the office of Naval Research and by the Advanced Sensors Application Program (ISSO), Department of Defense through Lawrence Livermore National Laboratory.

R. S. Awadallah is with the Applied Physics Laboratory, Johns Hopkins University, Laurel, MD 20723-6099 USA.

G. S. Brown is with the Bradley Department of Electrical Engineering, Virginia Polytechnic Institute and State University, Blacksburg, VA 24061–0111 USA.

Publisher Item Identifier S 0018-926X(00)09381-9.

Under the conditions of predominant forward propagation and scattering, i.e., when the rough surface is gently undulating and the angles of propagation and scattering are close to grazing, the one-way PWE approximation model proved to be very adequate [1]. An excellent account of the mathematical derivation of the PWE along with a detailed discussion of the underlying assumptions and approximations can be found in [2]. There are two levels of approximation used in the PWE method: the narrow-angle and the wide-angle approaches. Both of these formalisms neglect backscatter. The narrow-angle approximation is amenable to the very fast and efficient split-step Fourier method, however, its accuracy deteriorates as the solution region is moved away from the forward direction of propagation. The wide-angle approximation can more accurately predict propagation outside the forward region. Although most of the available forms of the wide-angle PWE require finite-difference solution, the form suggested by Thomson and Chapman [3] is amenable to the split-step Fourier method. A narrow-angle PWE/split-step model for studying low grazing angle (LGA) propagation over a rough surface was suggested in [4] among others. The great advantage of the PWE methods is that they can model most real-life nonhomogeneous environments. The drawback is the underlying paraxial approximation. Due to this approximation, the traditional PWE methods are only capable of modeling continuous forward multiple interactions on the rough surface. By contrast, the BIE method based on the two-way Helmholtz wave equation rigorously models all the surface field interactions. Provided the Green's function is known in an appropriate domain, an integral equation can be written for the currents induced on a perfectly conducting rough surface. These currents are then used in radiation integrals involving the appropriate propagators to calculate the scattered field at a point above the surface. Recently, a very elegant approach that combined the efficiency of the split-step method and the rigorousness of the BIE method and showed that the PWE methods have the potential to model forward/backward interactions was proposed by Rino and Ngo [5]. Nevertheless, the results reported in [5] are strictly forward-scattering results. It is worthwhile mentioning that PWE-based boundary integral equations models are also available in the literature. Uscinski [6] realized that for a medium with a linear sound-speed profile, the Green's function governed by the narrow-angle PWE can be evaluated using path integral techniques. He then used this Green's function in a PWE-based boundary integral equation formulation to study acoustic wave propagation over a rough surface in such medium. The same idea was used by Uscinski

0018–926X/00$10.00 © 2000 IEEE

to study high frequency acoustic propagation in shallow water [7]. The BIE models involved in our study are those based on the exact Helmholtz wave equation. The applicability of the BIE model is tied to the calculation of the Green's function for the medium of interest. There is, of course, no difficulty in this respect for a homogeneous medium. For nonhomogeneous media, exact closed-form integral expressions of the Green's function can be obtained for a small class of refractive index profiles. For general slowly varying profiles, approximate integral expressions of the Green's functions can be obtained via the WKB method [8]. The evaluation of the integrals involved in these Green's functions is not tractable numerically due to rapidly oscillating integrands. In this case, asymptotic methods of integration are the only resort.

In this paper, we use the BIE model to study the scattering from a rough surface in an infinite duct formed by a linear-square refractive index profile $n^2(z) = 1 - \varepsilon z$, where ε is a constant called the ducting parameter, where the Green's function can be written in terms of Airy functions [3]. We limit ourselves to such a medium which already gives useful insights into the problem of scattering by a rough surface in a ducting environment. The generalization of the method to more general environments will be the subject of a future study. We use asymptotic techniques to facilitate the computation of the Green's function and make it numerically tractable.

In the proposed BIE model, the surface currents are solved for via the method of ordered multiple interactions (MOMI). This method was developed by Kapp and Brown [9] and independently by Holliday *et al.* [10] who gave it the name forward-backward. MOMI is a robust and efficient iterative technique, which, as opposed to the traditional method of moments (MoM), does not require matrix storage and, hence, facilitates the application of the BIE method to very long rough surfaces. The proposed BIE/MOMI method is capable of predicting scattering in all directions including backscattering. This method is used to calculate the scattering from a variety of rough surfaces, including sinusoidal surfaces, surfaces with Gaussian roughness spectrum and surfaces with Pierson–Moskowitz roughness spectrum, in a ducting environment. Some results are compared to those produced by the narrow-angle PWE/split-step method. The ducting effects on the rough surface backscatter are also investigated in this paper.

II. Green's Function of a Line Source in an Infinite Medium with a Linear-Square Refractive Index Profile

The Green's function for the scalar Helmholtz equation in a medium with a linear-square refractive index profile of the form

$$n^2(z) = 1 - \varepsilon z \tag{1}$$

where ε is a constant called the ducting parameter, is given by [3] (please see (2) at the bottom of the page). In (2), $H = (\varepsilon k_o^2)^{-1/3}, t = t_o + z/H, t' = t_o + z'/H, t_o = H^2(\eta^2 - k_o^2)$, (x', z') is the source point, (x, z) is the field point, $A_i(\cdot)$ is the Airy function of the first kind, $B_i(\cdot)$ is the Airy function of the second kind, and k_o is the free-space wavenumber.

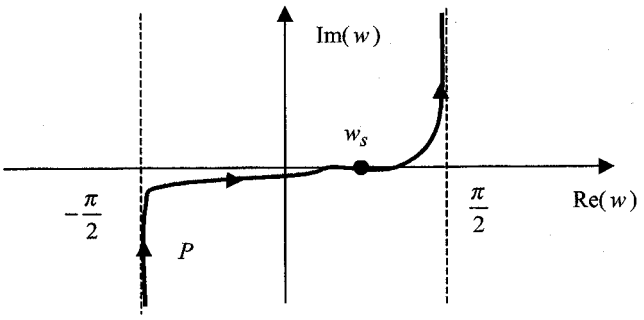

Fig. 1. Path of integration in the complex w plane.

The exact Green's function given by (2) is not numerically tractable since the integrals involved are difficult to evaluate even numerically due to the oscillatory nature of the integrands. Consequently, an approximate solution valid in the frequency range of interest, i.e., microwave range, is obtained asymptotically using the methods of steepest descents and stationary phase [8], [11]. To this end, we follow Felsen and Marcuvitz [8] and let

$$\eta = k_o \sin w \tag{3}$$

and notice that for large k_o, the Airy functions can be replaced by the leading term of their large argument asymptotic expansions, and hence, the integral in (2) can be written in the form

$$G = \frac{1}{4\pi j} \int_P dw\, f(w) \{\exp[-jk_o q_1(w)] + j \exp[-jk_o q_2(w)]\} \tag{4}$$

where P represents an appropriate contour of integration in the complex domain shown in Fig. 1. In (4)

$$f(w) = \frac{\cos w}{\{(1 - \varepsilon z - \sin^2 w)(1 - \varepsilon z' - \sin^2 w)\}^{1/4}} \tag{5}$$

$$q_1(w) = \sin w(x - x') + \int_{z_<}^{z_>} \sqrt{n^2(z) - \sin^2 w}\, dz \tag{6}$$

$$q_2(w) = \sin w(x - x') + \int_z^{z_t} \int_{z'}^{z_t} \sqrt{n^2(z) - \sin^2 w}\, dz \tag{7}$$

where $z_> = \max(z, z'), z_< = \min(z, z')$, z_t is known as the turning point and is defined as the point at which the equation $1 - \varepsilon(z \text{ or } z') - \sin^2 w = 0$ is satisfied.

One observes that using the large argument expressions of the Airy functions and their derivatives replaces the exact integrands of (2) by the WKB approximate ones given in (4). The

$$G(x, x', z, z') = \frac{H}{2} \begin{cases} \int_{-\infty}^{\infty} [B_i(t') - jA_i(t')] A_i(t) e^{-j\eta(x - x')}\, d\eta, & z > z' \\ \int_{-\infty}^{\infty} A_i(t') [B_i(t) - jA_i(t)] e^{-j\eta(x - x')}\, d\eta, & z < z' \end{cases} \tag{2}$$

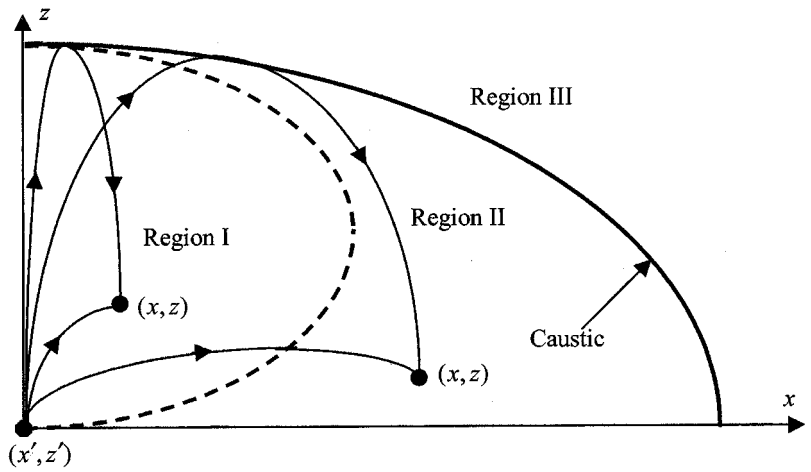

Fig. 2. Ray picture of the Green's function.

WKB approximation is a good one for slowly varying refractive index profile, i.e., $|dn/dz/k_o n^2| \ll 1$ [8]. It is applicable in the case at hand, where $n^2 \cong O(1), |dn/dz| \cong O(\varepsilon)$ and the frequency of interest is in the microwave range. This also says that our method is applicable for any slowly varying refractive index profile where we can easily write the WKB solution. Furthermore, although the value $\varepsilon = 0.0001$ was chosen in this work, a smaller and more realistic value of ε makes the approximations incurred in our development more accurate.

The asymptotic evaluation of the integral in (4) is carried out in three different regions in space [8]. These regions are delimited in Fig. 2. In region I, each observation point is reached by two eigenrays. The first ray propagates directly from the source to the observation point and is characterized by the stationary point $w_{s_{11}}$ obtained by solving $[dq_1/dw]_{w=w_{s_{11}}} = 0$. As exhibited in Fig. 2, this ray propagates from the source to the observation point while undergoing continuous refraction and manages to reach the observation point without having to reverse its direction under the influence of refraction. In this paper, this ray is called the direct ray. The second ray, which is characterized by the stationary point $w_{s_{12}}$ obtained by solving $[dq_2/dw]_{w=w_{s_{12}}} = 0$, propagates again under continuous refraction, all the way to the caustic and then gets reflected toward the observation point. This ray is called the caustic-reflected ray. The contribution of each stationary point to the integral in (4) is evaluated and the results are added to obtain the Green's function in this region. In region II, the direct rays mentioned above reach the observation points after undergoing a direction reversal under the influence of refraction (see Fig. 2). These rays are called refracted rays and are characterized by the stationary points $w_{s_{21}}$ obtained by solving $[dq_2/dw]_{w=w_{s_{21}}} = 0$. The caustic-reflected rays continue to exist in this region and they are characterized by the stationary points $w_{s_{22}}$ obtained by solving $[dq_2/dw]_{w=w_{s_{22}}} = 0$.[1] Regions I and II are separated in space by the curve [12]

$$(x - x') = \sqrt{\frac{4}{\varepsilon}(z - z')(1 - \varepsilon z)}. \tag{8}$$

[1]In region II, $[dq_2/dw]_{w=w_s} = 0$ has two roots.

As long as the points $w_{s_{21}}$ and $w_{s_{22}}$ are well isolated, the contribution of each of them to integral (4) can be evaluated independently and the results are added to obtain the Green's function in region II. When $w_{s_{21}} \to w_{s_{22}}$, the contribution of each one of them to the integral cannot be treated independently and the stationary phase procedure must be modified to accommodate two nearby stationary points [8], [11]. It can be shown that the stationary points are well isolated as long as

$$\left| -k_o^{2/3}\sigma \right| < \delta \tag{9}$$

where

$$\sigma = \{(3/4)\left[q_2\left(w_{s_{22}}\right) - q_2\left(w_{s_{21}}\right)\right]\}^{2/3} \tag{10}$$

and δ is the minimum Airy function's argument that allows the replacement of the Airy function $A_i(\delta)$ with the leading term of its large argument asymptotic expansion [11]. The result given by the modified stationary phase for two nearby stationary points is also valid on the caustic where the two stationary points exactly coalesce and σ in (10) becomes exactly zero. In this case, $w_{s_{21}} = w_{s_{22}} = w_c$ is a second order stationary point which simultaneously satisfies the two equations

$$\left.\frac{dq_2(w)}{dw}\right|_{w=w_c} = 0 \tag{11}$$

$$\left.\frac{d^2q_2(w)}{dw^2}\right|_{w=w_c} = 0. \tag{12}$$

The elimination of w_c from (11) and (12) yields the caustic curve

$$\xi(x, z) = 0 \tag{13}$$

which separates the regions II and III.

In the theory of geometrical optics, the caustic is the defined as the boundary between the propagation and the shadow regions. In region III, stationary points $w_{s_{21}}$ and $w_{s_{22}}$ separate from each other, move into the complex plane, and form a complex conjugate pair. In this case we resort to the method of steepest descents and determine the Green's function by analytically continuing the Green's function obtained on the caustic into the complex domain [8]. Since region III coincides with the

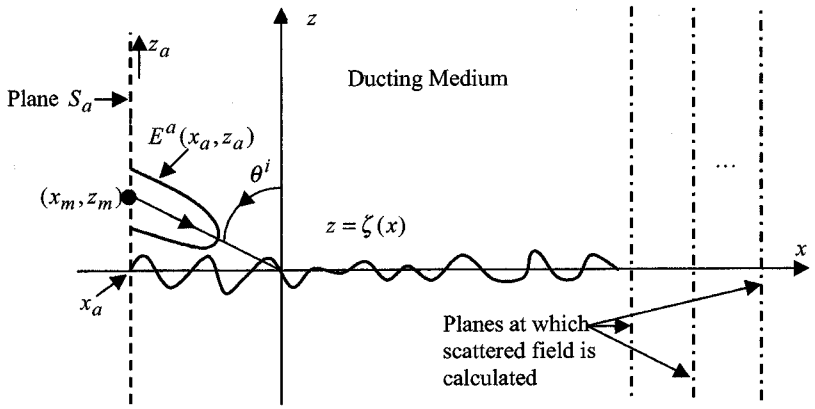

Fig. 3. Problem geometry.

shadow region, we expect our Green's function to be exponentially decaying there and indeed it is so.

Together, Regions I and II form the largest portion of the propagation region. In these regions, the caustic-reflected ray exists as a byproduct of the fact that the refractive index profile under consideration is monotonically decreasing with height. This means that eventually, the refractive index profile will pass through zero and attain a negative value at a certain height beyond which no propagation is permitted and the field is totally evanescent. In many physical ducting environments, the refractive index profile decreases with height up to a certain point and eventually reaches a constant value. In such environments, the steep rays, which in our model reach the caustic before getting bent down by refraction, escape the duct and do not contribute to the ducted field. The modeling of such environments via the method presented in this paper will be the subject of a future study. For now, the nonphysical contribution of the caustic-reflected rays to the field can be eliminated by eliminating the contribution of the stationary point which gives rise to it in the Green's function integral (4). The effect of the caustic reflections will be demonstrated in one of the numerical examples in Section VI.

We should mention here that, as pointed out in [8], the major contribution to integrals like the one in (4) comes from the neighborhood of the stationary (saddle) points either at large observation distances or for short wavelengths. This is to say that the normalized distance $|\vec{r} - \vec{r}'|/\lambda_o$ must be large enough for the steepest descent or stationary phase method to yield accurate results. Evidently, these methods are sufficiently accurate for microwave frequencies especially for observation points located in the far-field region.

III. Magnetic Field Integral Equation Formulation of 2-D Scattering Problems and the Method of Ordered Multiple Interactions

The BIE used to model the scattering problem in this paper is the magnetic field integral equation (MFIE). In this section, we recall the principles of MFIE/MOMI as applied to the problem of LGA electromagnetic wave scattering from a one-dimensional (1-D) randomly rough perfectly conducting surface located in a duct formed by a linear-square refractive index profile. The MFIE governing the current induced on a conducting rough surface by an incident field is set up and numerically solved using MOMI.

As exhibited in Fig. 3, we elected to work with Cartesian coordinates, where the x-axis extends along the mean plane of the rough surface and the single-valued surface height above the mean plane is given by the function $z = \zeta(x)$. In Fig. 3, θ_i is the angle of incidence, the point $(x_m, z_m = x_m \tan(\pi/2 - \theta_i))$ represents the center of the initial field beam, $E^a(x_a, z_a)$. This field is propagated toward the rough surface to obtain the incident field $E^i(x, z)$. The vertical dash–dotted lines, in Fig. 3, represent the range vertical planes at which the scattered field is to be calculated via the appropriate radiation integrals involving the surface currents.

The MFIE for an infinite perfectly electric conducting (PEC) rough surface has the form [13]

$$J(x) = J^i(x) + \int_X P(x, x') J(x')\, dx' \tag{14}$$

where

$J(x)$	unknown surface current;
$P(x, x')$	propagator;
$J^i(x)$	"Kirchhoff current" induced on the surface by the incident field.

The domain of integration X in (14) is infinite in principle, however, it can be made finite by using an appropriately tapered incident field. For TE waves, i.e., when the incident electric field E^i is tangential to the surface, the quantities involved in (14) are given by

$$J^i(x) = 2\frac{\partial E^i(x, z)}{\partial n}\bigg|_{z=\zeta(x)} \tag{15}$$

$$J(x') = \frac{\partial E(x', z')}{\partial n'}\bigg|_{z'=\zeta(x')} \tag{16}$$

$$P(x, x') = -2\frac{\partial G(x, x')}{\partial n}\sqrt{1 + \zeta_x^2(x')}. \tag{17}$$

For TM waves, i.e., when the incident magnetic field H^i is tangential to the surface, the above quantities are defined as follows:

$$J^i(x) = 2H^i(x, z)|_{z=\zeta(x)} \tag{18}$$

$$J(x') = H(x', z')|_{z'=\zeta(x')} \tag{19}$$

$$P(x,x') = 2\frac{\partial G(x,x')}{\partial n'}\sqrt{1+\zeta_x^2(x')}. \tag{20}$$

In (15)–(20), $G(x,x')$ is the Green's function propagator that was derived in the previous section, $\partial/\partial n$ is the derivative along the surface normal at a given point, E and H are the total electric and magnetic fields on the surface. The factor $\sqrt{1+\zeta_x^2(x')}$ results from converting the integral along the rough surface into an integral along the mean surface plane and $\zeta_x(x)$ is the surface slope at the point x. The scattered field E^s for the TE case can be determined by

$$E^s(\vec{r}) = \int_X G(\vec{r},x',z'=\zeta(x'))J(x')\sqrt{1+\zeta_x^2(x')}\,dx'. \tag{21}$$

For the TM case, the scattered field H^s is given by

$$H^s(\vec{r}) = \int_X \frac{\partial G(\vec{r},x',z'=\zeta(x'))}{\partial n'}J(x')\sqrt{1+\zeta_x^2(x')}\,dx'. \tag{22}$$

For an arbitrary surface, the MFIE can only be solved numerically. To this end, (14) must be discretized and put in the following matrix form:

$$J = J^i + PJ \tag{23}$$

where J is now a vector that contains the total surface current sampled at a uniform grid of N discrete points $\{x_m\}$ with a sample spacing of Δx, J^i is another vector that contains the Kirchhoff current sampled at the same discrete points $\{x_m\}$, and P is a square propagator matrix, with entries $P_{mn} = P(x_m,x_n)\Delta x$ which accounts for interactions between the different current elements on the surface. The classical MoM solution to (23) is given by

$$J = (I-P)^{-1}J^i. \tag{24}$$

This requires the storage and inversion of the matrix $(I-P)$ either directly or via the LU decomposition. This procedure becomes numerically prohibitive when the illuminated area on the rough surface is large. This difficulty is alleviated by MOMI as follows. The propagator matrix P is split into the lower and upper triangular matrices L and U; $P = L+U$. It can then be shown [9] that the discretized integral equation (23) can be recast into the following form:

$$J = (I-U)^{-1}(I-L)^{-1}J^i + (I-U)^{-1}(I-L)^{-1}LUJ \tag{25}$$

where I is the identity matrix. The first term in (25), given by

$$J_B \equiv (I-U)^{-1}(I-L)^{-1}J^i \tag{26}$$

is the so-called "new Born term." This term can be used to iterate (25). It serves as the zeroth-order iterate in the solution of (25) given by [9]

$$J = \sum_{n=0}^{\infty}\{(I-U)^{-1}(I-L)^{-1}LU\}^n J_B. \tag{27}$$

Due to the triangular nature of the matrices $(I-L)$ and $(I-U)$, no matrix inversion is required to compute the "new Born term" or any of the higher order iterates. Instead, forward or back substitution can be used. This eliminates the necessity to store and invert the propagator matrix as required by the classical MoM. As a matter of fact, it turns out that in many practical cases involving rough surface scattering, the new Born term by itself produces accurate results and it is not necessary to go to higher order iterates. The computation time necessary to calculate the new Born term goes like $N^2 - N$ and, thus, a considerable savings is achieved over the LU decomposition method used to invert the matrix in MoM solution for which computation time goes like $N^3/3 + N^2 - 5N/6$. In this paper, we are dealing with LGA rough surface scattering. As the angle of incidence approaches grazing, the illuminated surface area becomes larger, which means that the number of samples N used to represent the surface current gets larger and the classical MoM approach becomes prohibitive, while MOMI provides a much more promising alternative.

IV. The Incident Field

The incident field, which appears in the MFIE, is defined as the field produced by the source (antenna) that would exist in the medium in the absence of the rough surface. When the BIE/MOMI approach is used to simulate the problem of propagation over a rough surface in a ducting medium, it is appropriate to calculate the field produced by the source—the initial field—on a certain vertical plane S_a. The incident field on the rough surface, E^i in the TE case and H^i in the TM case is then evaluated by propagating the initial field from the vertical plane onto the rough surface using the ducting medium propagator. We use an initial field constructed from an angular spectrum of plane waves of the form [14] (see Fig. 3)

$$\psi^a(x_a,z_a) = \frac{1}{\sqrt{\pi}\Delta\theta}\int_{-\pi/2}^{\pi/2} e^{-[(\theta-\theta^i)^2/(\Delta\theta)^2]} \times \exp[-jk_o(x_a\sin\theta - z_a\cos\theta)]\,d\theta. \tag{28}$$

In (28)

- ψ^a represents the initial fields: E^a for the TE case and H^a for the TM case;
- θ_i is the angle of incidence measured from the positive z-axis;
- $\Delta\theta = 2/k_o g\cos\theta_i$;
- g is the half-beam waist;
- The center of the beam is located at $(x_m = x_a, z_m = \tan(\pi-\theta_i)x_m)$.

If the integration in (28) is performed in an exact manner, the above incident field satisfies Maxwell's equations exactly. The "Kirchhoff" current J^i, which appears in the MFIE (14), is given by

$$J^i(x) = 2\frac{\partial E^i(x,z)}{\partial n}\bigg|_{z=\zeta(x)} = 4\int_{S_a}\frac{\partial E^a}{\partial n_a}\left[\frac{\partial G(x_a,x,z_a,z)}{\partial n}\right]_{z=\zeta(x)} dz_a \tag{29}$$

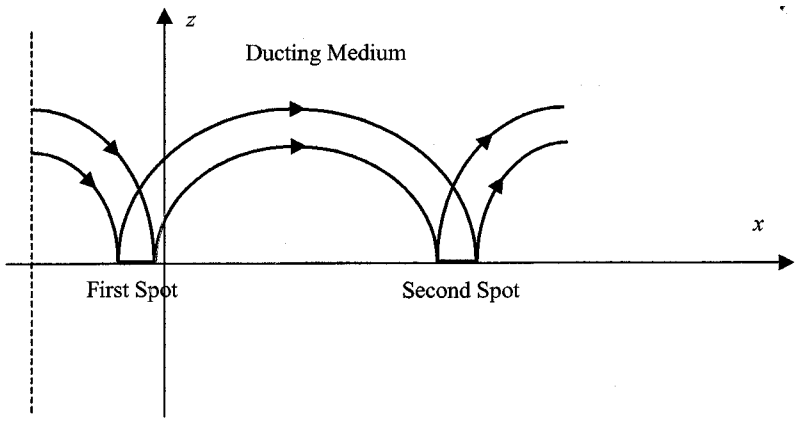

Fig. 4. Multiple bounces of the specular field in a ducting environment.

for the TE case and

$$J^i(x) = 2H^i(x,z)|_{z=\zeta(x)} = 4\int_{S_a} H(x_a,z_a) \times \left[\frac{\partial G(x_a,x,z_a,z)}{\partial n_a}\right]_{z=\zeta(x)} dz_a \qquad (30)$$

for the TM case. In (29) and (30), $\vec{n}_a = \hat{x}$ is the normal vector to the vertical plane $S_p, \vec{n}$ is the normal to the rough surface and G is the Green's function derived in Section II for a ducting medium characterized by a linear-square refractive index profile.

In rough surface scattering calculations, tapered fields are used to limit the size of the rough surface area illuminated by the incident field and hence make the numerical computations based on MoM tractable. As the angle of incidence approach grazing, this illuminated area grows larger and larger and as a result, the size of the matrices that need to be stored and inverted to obtain the MoM solutions becomes prohibitive. This problem is alleviated by MOMI as was mentioned earlier. However, MOMI is still a $O(N^2)$ procedure and, hence, although it is feasible for large illuminated areas, its efficiency deteriorates as N becomes very large. For homogeneous space, Chou and Johnson [15] proposed a $O(N)$ novel acceleration algorithm for the forward–backward method or MOMI. Their method is based on a new expansion of source current elements via a spectral-domain representation of the Green's function. For the inhomogeneous environments considered in this paper, analogous methods of improving the efficiency of MOMI are still under investigation. Although the tapered beam widths and, hence, the surface illuminated spots dealt with here are relatively small and hardly realistic for actual antennas, they certainly serve to illustrate the features of our method and are definitely out of the reach of a classical MoM approach.

V. Single-Bounce versus Multiple-Bounces Scattered Field

Throughout this paper, the field scattered by the currents induced by the incident field are termed the "single bounce" scattered fields. Due to ducting, the parts of the field scattered at very low angles are going to encounter the rough surface again and again in the form of multiple bounces. The surface current due to the multiple bounces of the scattered field can be calculated through the direct application of MOMI to the entire surface. This is feasible but not efficient due to the reasons mentioned in the previous section. For LGAs scattering of narrow tapered incident fields, most of the energy propagates in the forward direction where the specular field dominates. Knowing the specular angle $\theta_o = \theta_i$ and the angular width of the specularly scattered beam, $\Delta\theta_o$, allows the approximate calculation of the location of the second spot and its size via well-known geometrical optics formulas [16]. The width $\Delta\theta_o$ can be inferred from the single-bounce scattered field evaluated at a convenient range. This approximation saves us considerable time in the computation of the surface current. For the case of two illuminated spots, MOMI can be set up to calculate the surface currents induced on these different spots as follows. Consider the situation depicted in Fig. 4. As was outlined in Section III, the discretized integral equation governing the surface current is given by

$$J = J^i + PJ = J^i + (L+U)J. \qquad (31)$$

In the case of two illuminated spots, the lower triangular matrix, L, contains all the forward current interactions within each illuminated spot in addition to all forward interactions between the first and second illuminated spots through the refractive medium. The matrix U, on the other hand, contains all the backward interactions within each illuminated spot in addition to all backward interactions between the second and the first illuminated spots through the refractive medium. Since all the rough surfaces we are dealing with have maximum excursions that only deviate slightly from the $z = 0$ mean plane, the surface interactions within the same spot can be accounted for using the free-space propagator. However, it is obvious from Fig. 4 that the interspot surface interactions must be accounted for via the ducting medium propagator. Again this is an approximation. For the more realistic cases of wide incident beams or actual antenna patterns, this multiple spot approximation is no longer accurate and the entire surface must be taken into consideration when solving for the surface currents.

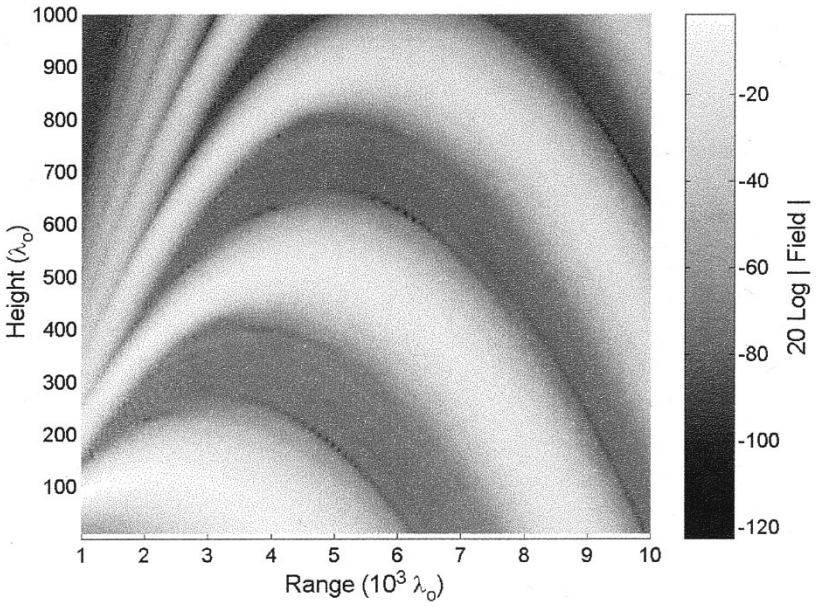

Fig. 5. Magnitude (decibels) of the single-bounce field scattered by a sinusoidal surface in a ducting environment ($\theta_i = 85°, g = 200\lambda_o, L = 1000\lambda_o$, TE polarization).

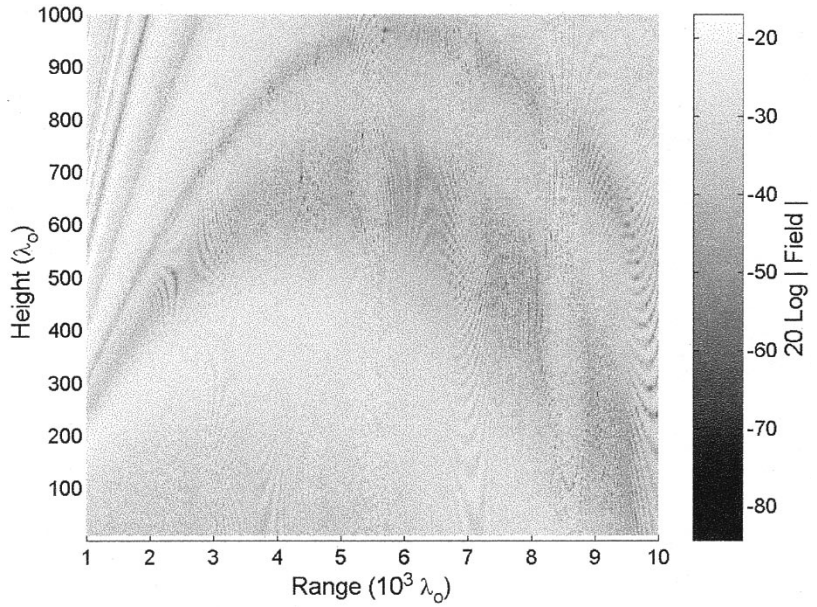

Fig. 6. Magnitude (decibels) of the single-bounce scattered field from a single realization of a surface with Gaussian roughness ($\theta_i = 80°, h = 0.5\lambda_o, l = 2\lambda_o, L = 300\lambda_o, g = 40\lambda_o, x_a = -500\lambda_o$, TM polarization).

VI. Results and Discussion

Having determined the Kirchhoff surface current, MOMI can be used to solve for the surface current induced by the incident field on different types of rough surfaces. Knowing the current induced on the rough surfaces, the field scattered inside the ducting medium can then be determined using the radiation integrals given by (21) and (22) for the TE and TM case, respectively.

In this section, the BIE/MOMI method is applied to the problem of scattering from different types of surfaces, namely sinusoidal surfaces, surfaces with a Gaussian roughness spectrum and surfaces with a Pierson–Moskowitz roughness spectrum. Unless otherwise indicated, only single bounce scattered fields are calculated in this section. Some examples with multiple field bounces on the rough surface are presented later on in this section. Also, numerical computations are carried out for single surface realizations unless otherwise indicated. For all the numerical simulations presented in this paper, the sampling interval, Δx, is chosen to be $0.1\lambda_o$ while the ducting parameter, ε is chosen to be 0.0001. As the first example, we consider scattering from a sinusoidal surface given by

$$\zeta(x) = A + A\cos k_s x \tag{32}$$

where $A = (1.5/\pi)\lambda_o$ and $k_s = 2\pi/50\lambda_o$. In this example, $x_a = -500\lambda_o, \theta^i = 85°, g = 200\lambda_o$, the surface length (L)

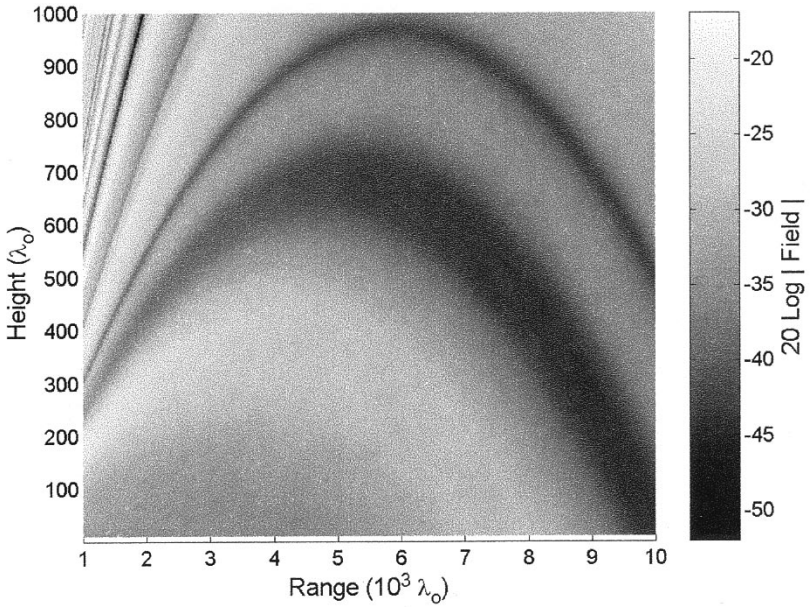

Fig. 7. Magnitude (decibels) of the single-bounce scattered field of Fig. 7 with the caustic-reflected field eliminated.

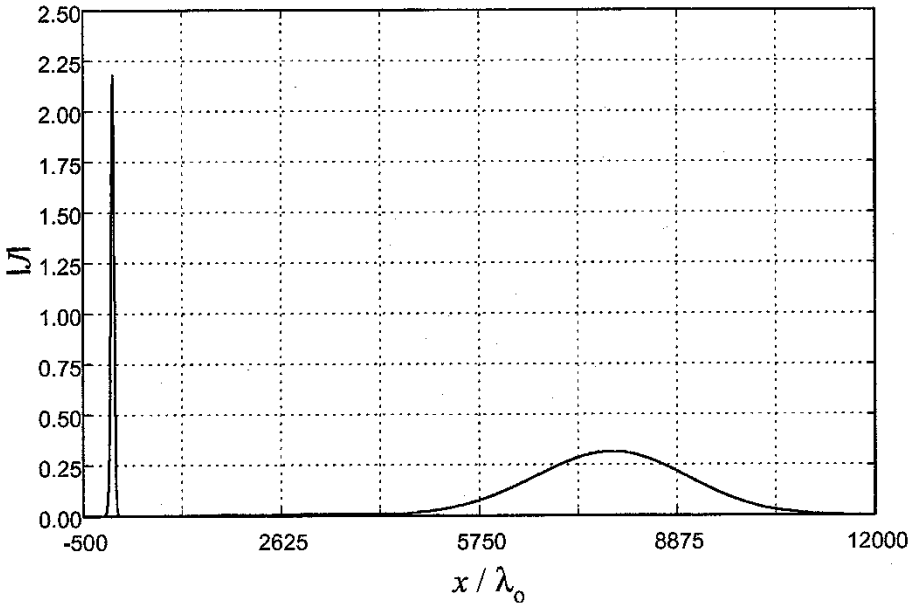

Fig. 8. Magnitude of the surface current induced on two illuminated spots of a flat surface. ($\theta_i = 80°, g = 40\lambda_o, x_a = -500\lambda_o, L = 12\,500\lambda_o$, TE polarization).

is $1000\lambda_o$ and the polarization is horizontal (TE). The surface length L is used in calculating the initial induced currents on the surface. The single-bounce field scattered by the above surface in the ducting medium is exhibited in Fig. 5. In the second example, we demonstrate the effect of the caustic-reflected rays by considering the scattering from a very rough surface with a Gaussian roughness spectrum. The root mean square (rms) height (h) of this surface is $0.5\lambda_o$ and the correlation length (l) is $2\lambda_o$. Other parameters in this example are the following: $\theta_i = 80°, L = 300\lambda_o, x_a = -500\lambda_o$ and $g = 40\lambda_o$. The polarization in this example is vertical (TM). With the contribution of the caustic-reflected rays to the Green's function taken into account, the single-bounce field scattered by the above surface into the ducting environment is shown in Fig. 6. The interference between the caustic-reflected and the refracted/scattered fields is clearly demonstrated in this figure. Fig. 7, on the other hand, exhibits the interference-free refracted/scattered field for the same example above obtained by eliminating the caustic-reflected ray contribution to the Green's function.

Next, we consider two examples illustrating the application of the approximate method of treating multiple illuminated spots outlined in Section V. The first of these is for a flat surface. The parameters in this example are the following: $\theta^i = 80°, g = 40\lambda_o, x_a = -500\lambda_o$ and the polarization is TE. The surface current on the two illuminated spots is shown in Fig. 8. We observe that the shape of the surface current on the second illuminated spot is still Gaussian with a beam waist which is much larger than that of the current on the first illuminated spot. The

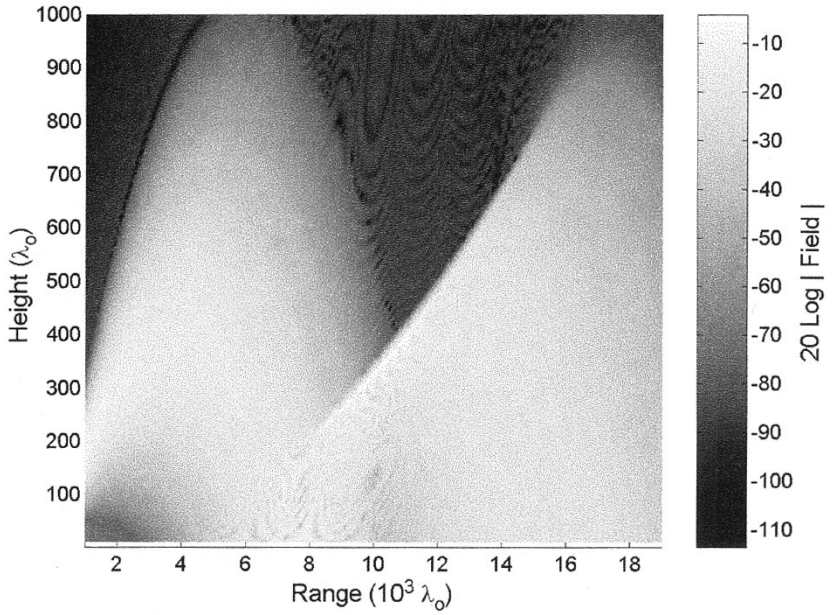

Fig. 9. Magnitude (decibels) of the scattered field due to the surface current induced on two illuminated spots of Fig. 8.

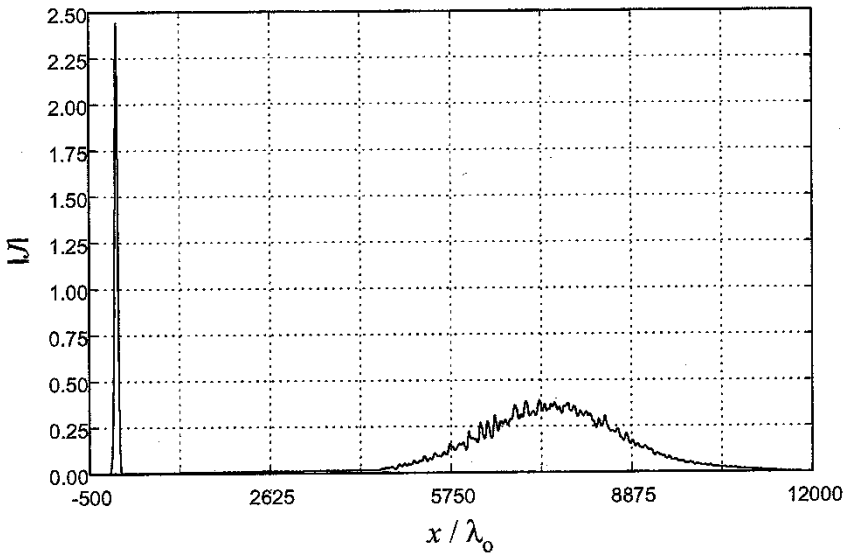

Fig. 10. Magnitude of the surface current induced on two illuminated spots of a Gaussian surface. ($\theta_i = 80°, g = 40\lambda_o, x_a = -500\lambda_o, L = 12\,500\lambda_o, h = 0.5\lambda_o, l = 50\lambda_o$, TE polarization).

scattered field due to both current spots is shown in Fig. 9. Due to its narrow beamwidth localized around $\theta^i = 80°$, the incident field on the first spot results in well-defined reflected field. The medium inhomogeneity causes this narrow beam to widen upon scattering from the surface. Consequently, the field that impinges on the second spot is no longer localized around the specular direction. This means that different parts of this field impinge on the surface at different angles, which results in a wide variation of specular reflection angles; the interference between these reflected fields gives rise to the pattern shown in Fig. 9. This same example is repeated for a slightly rough Gaussian surface with rms height of $0.5\lambda_o$ and a correlation length of $50\lambda_o$. Fig. 10 shows the surface currents induced on the two illuminated spots of the rough surface for this example. Fig. 11 shows the scattered field due to the surface currents on the two illuminated spots of the Gaussian surface in the above example. From this figure, it is obvious that the rough surface encountered at the second illuminated spot gives rise to a diffuse scattered field. One observation from Figs. 9 and 11 is that due to the widening of the specular field under the influence of refraction, the second and third illuminated spots are not well separated. Hence, our approximate method of handling multiple spots is not accurate beyond the second illuminated spot and the entire surface must be considered thereafter.

The BIE/MOMI is capable of accurately predicting scattering in all directions including the backscattering direction. Fig. 12 shows the magnitude of the "one bounce" scattered field from a Pierson–Moskowitz surface charac-

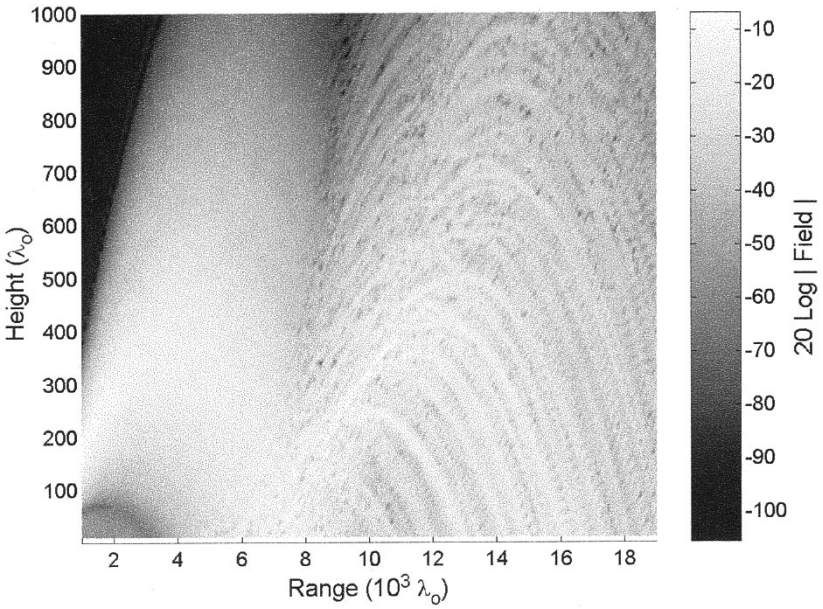

Fig. 11. Magnitude (decibels) of the scattered field due to the surface current induced on two illuminated spots of Fig. 10.

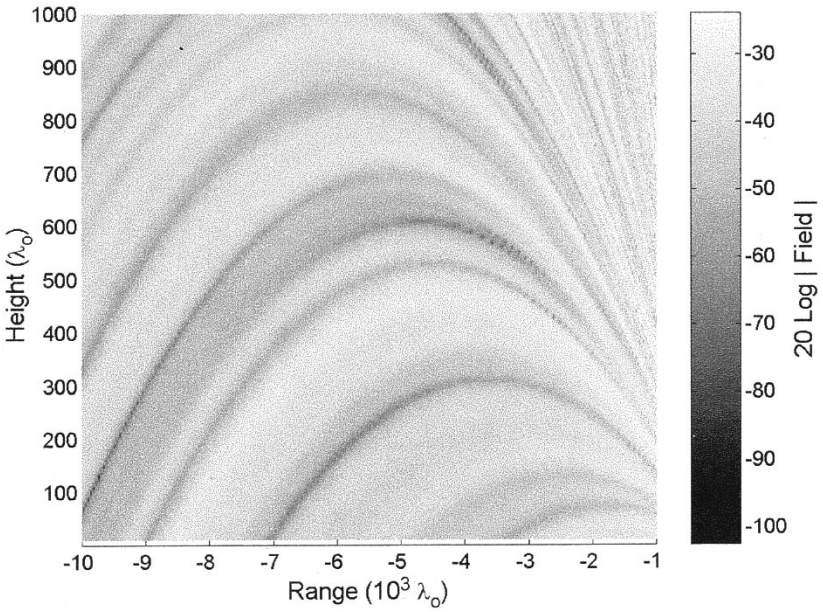

Fig. 12. Magnitude (decibels) of the single bounce scattered field in the near backscattering direction from a single realization of a surface with a Pierson–Moskowitz roughness spectrum ($\theta_i = 85°, K_c = 5k_o, \lambda_o = 0.23$ m, $L = 1000\lambda_o, x_a = -500\lambda_o, g = 200\lambda_o$, TM polarization).

terized by a wind speed of 5 m/s and a cutoff wavenumber $K_c = 5k_o$ in the near backscattering direction for the TM case. Other parameters in this example are as follows: $\theta_i = 85°, x_a = -500\lambda_o, L = 1000\lambda_o, g = 200\lambda_o$ and $\lambda_o = 0.23$ m. One very important aspect of Fig. 12 is that, for a strong refractive index profile, the backscattered incoherent power calculated as a function of distance in the backscattering direction and along a constant scattering angle radial does not have the simple inverse distance dependence, but exhibits an oscillatory pattern on a realization by realization basis and reaches a certain smooth pattern upon averaging over many realizations. This is attributed to the fact that under the influence of refraction, the fields scattered in other near-backscattering directions contaminate the direct backscattered field. This effect is depicted in Fig. 13, where the average backscattered field over 100 realizations of the Pierson–Moskowitz surface in a ducting environment is compared with the same average calculated in homogeneous space. The effect of the refractive index profile is more pronounced on a realization by realization basis as shown in Fig. 13; however, this effect averages out when multiple realizations are considered. From Fig. 13, one observes that for observation points located at small distance from the origin, the average incoherent power is the same for the homogeneous and the ducting medium. This is due to the fact that the refraction effects are not prominent at such short ranges. The variability of the backscattered incoherent average power due to refraction might be of importance in inverse scattering applications where information about the refractive

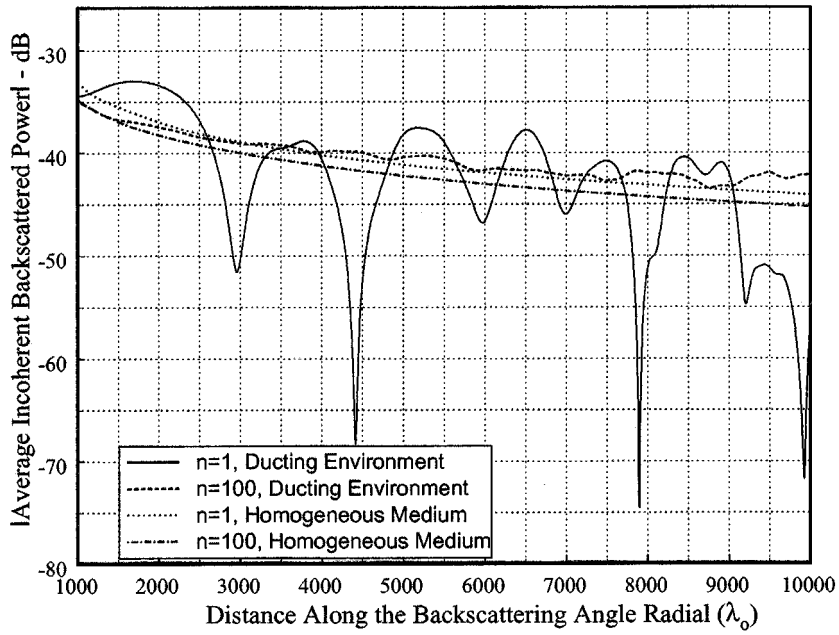

Fig. 13. Magnitude of the average incoherent single bounce backscattered power in a ducting environment versus that of a homogeneous medium. ($\theta_i = 85°, g = 140\lambda_o, v = 5$ m/s, $K_c = 2k_o, \lambda_o = 0.23$ m, $x_a = -500\lambda_o, n$: number of surface realizations, TM case).

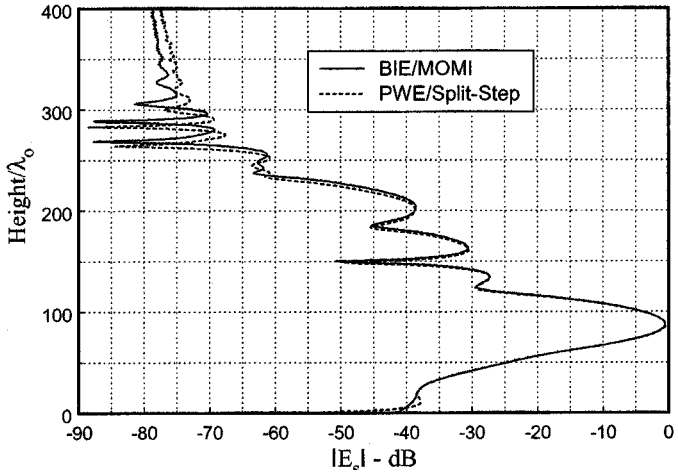

Fig. 14. Magnitude of the "one bounce" scattered field obtained using the BIE/MOMI approach versus that obtained using the PWE/split-step approach for a Gaussian surface. The field is evaluated at a vertical plane located at the range point $x = 1000.05\lambda_o$ ($\theta_i = 85°, g = 200\lambda_o, L = 1000\lambda_o, h = 0.1\lambda_o, l = 44.72\lambda_o$, TE polarization).

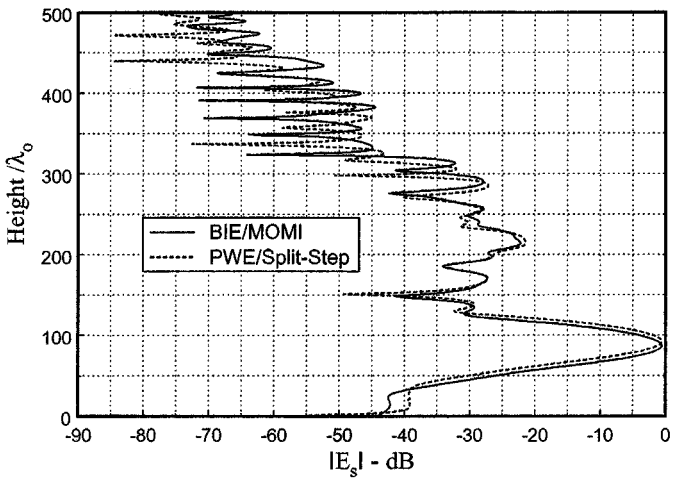

Fig. 15. The scattered field of Fig. 17 with l changed to $14.142\lambda_o$.

index profile is inferred from the statistical parameters of the measured backscatter data in the ducting environment.

The next few examples present some comparisons between the BIE/MOMI method and the narrow-angle PWE/split-step method. The surface roughness is incorporated in the PWE/split-step model via the appropriate coordinate transformations as in [4]. In the following examples, the horizontal step Δx in the PWE/split-step regime is chosen to be $0.1\lambda_o$. In Fig. 14, the single-bounce scattered field in the near forward direction from a gently undulating Gaussian rough surface as calculated by the BIE/MOMI method is compared to that calculated by the PWE/split-step method. This figure exhibits the magnitude of the scattered field calculated along the vertical plane located at $x = 1000.05\lambda_o$ from a Gaussian surface with a rms height of $0.1\lambda_o$ and a correlation length of $44.72\lambda_o$ due to an incident field of the form (28) which was defined on a vertical plane located at $x_a = -500\lambda_o$. Other parameters in this example are as follows: $\theta_i = 85°, g = 200\lambda_o, L = 1000\lambda_o$ and the polarization is TE. The solid curve represents the BIE/MOMI result while the dashed curve represents the PWE/split-step result. One notes that, for such a smooth surface, the agreement between the two results is good especially in the forward direction. However, when the same example above is repeated for a rougher surface where $h = 0.1\lambda_o$ and $l = 14.142\lambda_o$, the agreement between the two methods is not as close, as exhibited in Fig. 15. In Figs. 16 and 17, the field scattered by the sinusoidal surface described by (32)

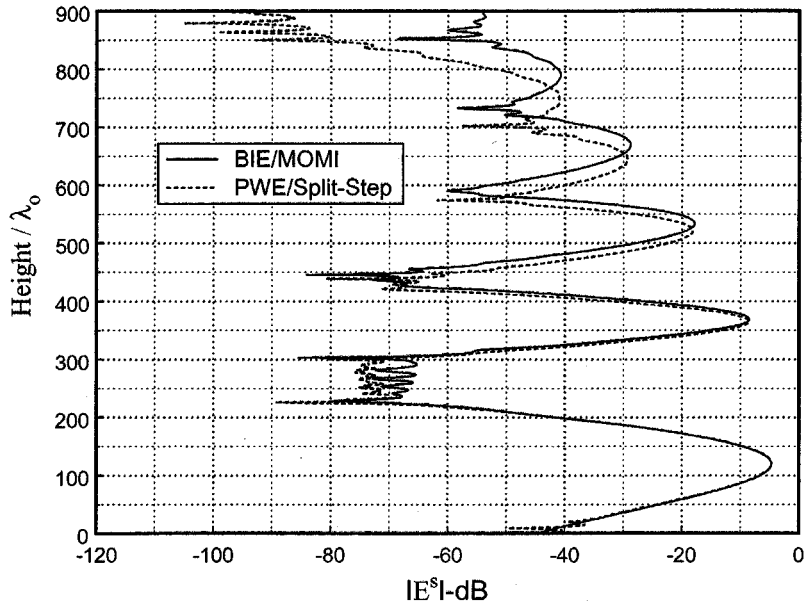

Fig. 16. Magnitude of the single-bounce scattered field obtained using the BIE/MOMI approach versus that obtained using the PWE/split-step approach for a sinusoidal surface. The field is evaluated at a vertical plane located at the range point $x = 2000\lambda_o$. ($\theta_i = 85°, g = 200\lambda_o, L = 1000\lambda_o, A = (1.5/\pi)\lambda_o, \Lambda = 50\lambda_o$, TE polarization).

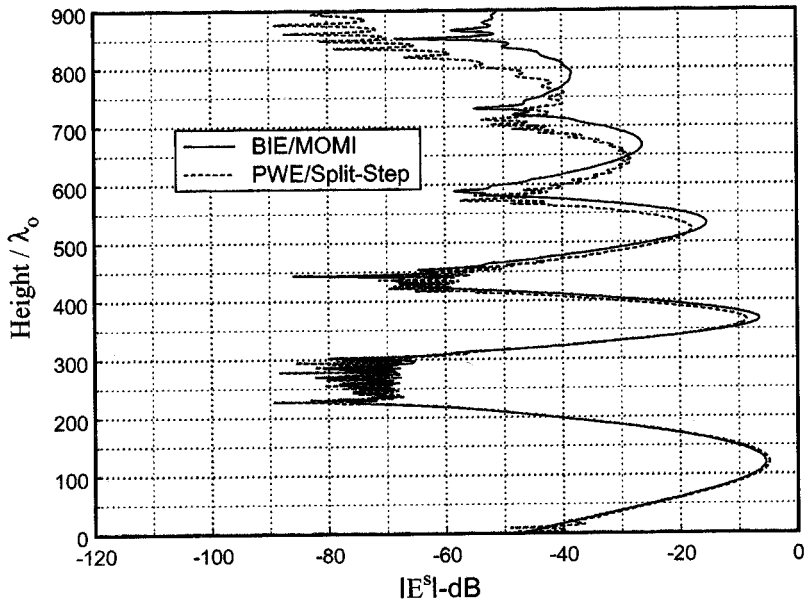

Fig. 17. The scattered field of Fig. 16 with the polarization changed to vertical (TM).

and obtained via the BIE/MOMI method is compared to that obtained via the PWE/split-step method for the TE and TM cases, respectively. The other parameters in this example match those of Fig. 5 and the scattered field is calculated on a vertical plane located at $x = 2000\lambda_o$ (see Fig. 3). These comparisons again show a good agreement between the two methods in the near forward direction. The agreement deteriorates as the scattering angle moves away from the forward direction. This is probably due to the fact that a narrow-angle PWE code has been used.

In the examples where the fields were computed in the two-dimensional (2-D) range-height plane we needed to work with shorter ranges than those used in radar applications, as our purpose was to illustrate the proposed method in an affordable amount of computation time. For smaller ε, the same 2-D plots can be generated at larger ranges and heights. For example, a ε value of one-tenth the one used in this paper give the same field configuration of that exhibited in Fig. 5, which covers a range of 30 km at a frequency of 1 GHz, while the existing Fig. 5 covers a range of 3 km at that frequency.

In realistic ducting environments, the value of ε is very small such that only the part of the field incident at angles very close to grazing are trapped by the duct. As mentioned earlier, the asymptotic technique used to evaluate the Green's function becomes more accurate for smaller ε, and hence the proposed method has no difficulty in that regard. However, at these very low grazing angle scenarios, large illuminated surface spots are inevitable and the serious problem faced by the proposed method is numerical efficiency. Methods of accelerating MOMI analogous to those proposed in homogeneous space, which were mentioned earlier in the text, are under investigation for inhomogeneous space. These methods will facilitate the application of the proposed method to very large surfaces and, hence, allow it to relate to the more realistic atmospheric propagation scenarios and makes it a more meaningful benchmark for the efficient PWE-based methods.

VII. Conclusion and Further Work

This paper documents the application of the rigorous BIE/MOMI method to the calculation of electromagnetic scattering from rough surfaces and propagation over rough terrain in a simple ducting environment characterized by a linear-square refractive index profile. Some comparisons between the results obtained using the BIE/MOMI method and those obtained via the narrow-angle PWE/split-step method display a good agreement between the two methods in the near-forward scattering direction when the surfaces under consideration are gently undulating. Although the combined effect of surface roughness and medium inhomogeneity is modeled by the BIE/MOMI method in a more rigorous fashion than the PWE/split-step method, the former method is not proposed as an alternative to the latter simply because it is not as efficient computationally. However, within the limitations discussed in the paper, which we hope to alleviate by applying acceleration techniques to MOMI, the BIE/MOMI method is meant to serve as a benchmark for the PWE-based methods. In addition, it provides a means by which the ducting effects on the scattered fields in directions not appropriately modeled or even neglected by the traditional PWE-based techniques, such as the backscattered field, can be investigated. One important item on our future work agenda is the generalization of the proposed method via the WKB method to more general refractive index profiles like the piecewise linear profiles which exist in many physical ducting environments. Another important item is the acceleration of MOMI in inhomogeneous space to allow the proposed method to handle very low-grazing angles, which mandates very large surface illuminated spots. A third item is the application of the proposed method to nonperfectly conducting surfaces on which an approximate impedance boundary condition is satisfied.

Acknowledgment

The authors would like to thank the other members of the ElectroMagnetic Interactions Laboratory for their suggestions and interest in the work. They would also like to thank Drs. R. Marchand and R. Adams for their invaluable technical assistance with the computing facility.

References

[1] F. D. Tappert, "The parabolic approximation method," in *Wave Propagation in Underwater Acoustics*, J. B. Keller and J. S. Papadakis, Eds. New York: Springer-Verlag, 1977, pp. 224–287.

[2] J. R. Kuttler and G. D. Dockery, "Theoretical description of the parabolic approximation/Fourier split-step method of representing electromagnetic propagation in the troposphere," in *Radio Sci.*, Mar.–Apr. 1991, pp. 381–393.

[3] F. B. Jensen, W. A. Kuperman, M. B. Porter, and H. Schmidt, *Computatational Ocean Acoustics*. New York: AIP, 1994, ch. 6.

[4] A. E. Barrios, "A terrain parabolic equation model for propagation in the troposphere," *IEEE Trans. Antennas Propagat.*, vol. 42, pp. 90–98, Jan. 1994.

[5] C. L. Rino and H. D. Ngo, "Forward propagation in a half-space with an irregular boundary," *IEEE Trans. Antennas Propagat.*, vol. 45, pp. 1340–1347, Sept. 1997.

[6] B. J. Uscinski, "Sound propagation with a linear sound-speed profile over a rough surface," *J. Acoust. Soc. Amer.*, vol. 94, no. 1, July 1993.

[7] ——, "High-frequency propagation in shallow water. The rough waveguide problem," *J. Acoust. Soc. Amer.*, pt. 1, vol. 98, no. 5, Nov. 1995.

[8] L. B. Felsen and N. Marcuvitz, *Radiation and Scattering of Waves*. New York: IEEE Press, 1994.

[9] D. A. Kapp and G. S. Brown, "A new numerical method for rough surface scattering calculations," *IEEE Trans. Antennas Propagat.*, vol. 44, pp. 711–721, May 1996.

[10] D. Holliday, L. L. DeRaad, and G. J. St-Cyr, "Forward-backward: A new method for computing low-grazing angle scattering," *IEEE Trans. Antennas Propagat.*, vol. 44, pp. 722–729, May 1996.

[11] V. A. Borovikov, *Uniform Stationary Phase Method*. London, U.K.: IEE Press, 1994, ch. 2.

[12] R. S. Awadallah, "Rough surface scattering and propagation over rough terrain in ducting environments," Ph.D. dissertation, Virginia Polytech. Inst. State Univ., 1998.

[13] J. V. Toporkov, R. T. Marchand, and G. S. Brown, "On the discretization of the integral equation describing scattering by rough conducting surfaces," *IEEE Trans. Antennas Propagat.*, vol. 46, pp. 150–161, Jan. 1998.

[14] E. Thorsos, "The validity of the Kirchhoff approximation for rough surface scattering using a Gaussian roughness spectrum," *J. Acoust. Soc. Amer.*, vol. 83, no. 1, pp. 78–92, Jan. 1988.

[15] H.-T. Chou and J. T. Johnson, "A novel acceleration algorithm for the computation of scattering from rough surfaces with the forward-backward method," *Radio Sci.*, vol. 33, no. 5, pp. 1277–1287, 1998.

[16] R. E. Collin, *Antennas and Radiowave Propagation*. New York: McGraw-Hill, 1985, sec. Appendix IV, pp. 480–482.

Ra'id S. Awadallah (S'97–M'98) was born in Jordan in 1966. He received both the B.S.E.E. in 1988 and M.S.E.E. degrees in 1988 and 1991, respectively, from the Jordan University of Science and Technology, Irbid-Jordan, and the Ph.D. degree in electrical engineering from Virginia Polytechnic Institute and State University, Blacksburg, VA, in 1998.

From 1991 to 1993, he worked as a Lecturer in the Department of Electronics in the Jerusalem University College of Sciences, Abu-Dis/Jerusalem. In 1998, he joined the Johns Hopkins University Applied Physics Laboratory, Laurel, MD, as a Research Associate where he is currently involved in a diversity of research areas including atmospheric propagation, electromagnetic scattering from randomly rough surfaces, ISAR imaging of complex air targets and, most recently, in optical imaging of sea surface. His research interests also include scattering from rough surfaces in ducting environments and mode coupling and filtering in waveguides with irregular boundaries.

Gary S. Brown (S'61–M'67–SM81–F'86) was born in Jackson, MS, on April 13, 1940. He received the B.S., M.S., and Ph.D. degrees from the University of Illinois, Urbana-Champaign, in 1963, 1964, and 1967, respectively.

From 1963 to 1967, he was a Research Assistant in the (former) Antenna Laboratory, University of Illinois, Urbana-Champaign, where he was involved with direction finding, shaped beam antennas, and millimeter waveguides. Whille in the U.S. Army Signal Corps (1967–1969), he served in an engineering capacity dealing with the Integrated Wide-Band Communications System (IWCS) in the Republic of Vietnam. During 1970, he was employed by TRW Systems Group, Redondo Beach, CA, where his work involved monopulse, electronic countermeasures, and multiple-beam antenna analysis and development. From 1971 to 1973, he was with the Research Triangle Institute, NC, where his primary area of interest was radar altimetry. From 1973 to 1985, he was employed by Applied Science Associates, Inc., Apex, NC, where he worked with microwave remote sensing, rough surface scattering, and propagation through random media. In 1985, he joined the faculty of Virginia Polytechnic Institute and State University, Blacksburg, VA, where he is presently Director of the ElectroMagnetic Interactions Laboratory (EMIL).

Dr. Brown is a member of Commissions B and F of USNC-URSI and is presently Secretary of the organization. He was President of the Antennas and Propagation Society in 1988 and received the R. W. P. King Award in 1978 and the Schelkunoff Best Paper Award (with J. Toporkov and R. Marchand) in 1999.